Maglev - Laboratory Project

Authors: Desmond Boateng, Pierre Gathy, Alex Citardi

Course: ME 344

Due Date: December 05, 2025

Authorship Contributions

- **Desmond Boateng:** Abstract, Introduction, Theory.
- **Pierre Gathy:** Obtaining Constants, Results, Conclusion
- **Alex Citardi:** VI design, Procedure, Results

1 Abstract

The main objectives of this laboratory project were to model, design, and implement a closed-loop control system that can levitate a steel ball using a Feedback Magnetic levitation (MagLev) device. To begin, a mathematical model of the nonlinear MagLev dynamics was developed, linearized about the equilibrium point, and key parameters were experimentally validated. These include the equilibrium current, I_0, equilibrium position, x_0, and the magnetic field constant, k. The linearized transfer function was then used to construct the theoretical block diagram, which guided the design of a PID controller to achieve performance specifications that allowed for stability in hovering and accurate performance tracking. The final controller achieved essentially zero steady-state error for a constant height input of 0.5 in. For random inputs with ± 0.15 in amplitude, the controller produces well-damped responses with small steady-state errors. The sinusoidal tracking remained accurate up to about 2 Hz with small phase lags. The square waves showed expected behavior, including rounded transitions and moderate overshoot, but the controller remained stable across all tested frequencies.
These results verify that a well-tuned PID controller can stabilize an unstable MagLev system and allow for accurate tracking of random reference inputs, such as sinusoids, constants, random, etc. However, there are several opportunities for improvements, including thinking of different control strategies, such as feedforward control with an inverse model, to reduce nonlinear effects, which will be looked at in the conclusion.

2 Introduction and Theory

2.1 Background on the Maglev System

The MagLev device (from station 3) used in this project is a single-input, single-output (SISO) system with model number 33-210 manufactured by Feedback Instruments Ltd. The device levitates a steel ball below an electromagnet, which has a coil controlled by a current regulated by a power amplifier. A photo-array sensor on the side measures the vertical position. Since the ball-magnet system operates on an open-loop unstable basis, any small deviation from the equilibrium will cause the ball to accelerate away from/towards the magnet. This explains why a controlled feedback system is needed for effective levitation, which will be discussed throughout the lab.

2.1.1 System Components

The MagLev device unit consists of three main parts:

1. **Electromagnet (the actuator):** This provided the upward magnetic force that opposes the gravitational force.
2. **Ball (the plant):** The object being controlled through the electromagnetic and gravitational forces.
3. **Photo-array Sensor (measurement):** This detects the ball height by converting the incident light into a voltage proportional to position.

The whole Maglev system and its main components are shown in Figures 1 and 2, respectively, below, referenced from the Lab Manual.

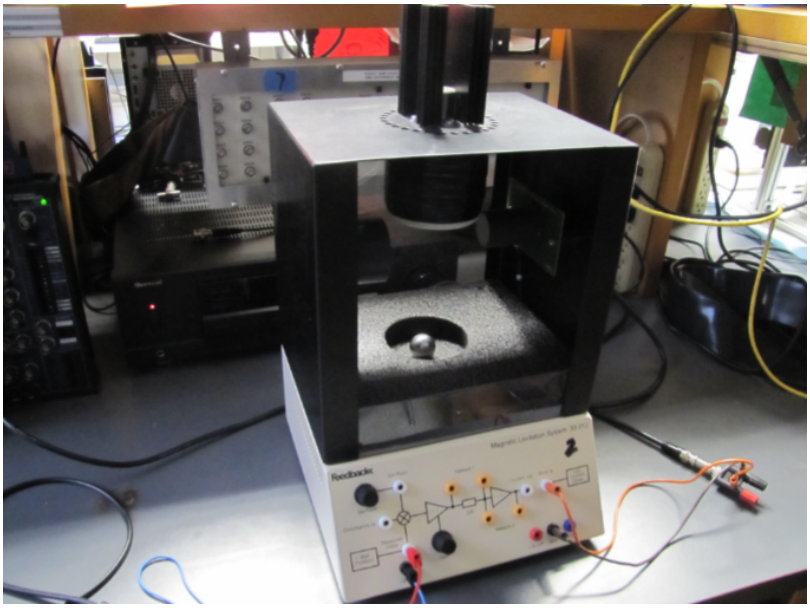

Figure 1: Isometric view of the MagLev device connected to the NI DAQ

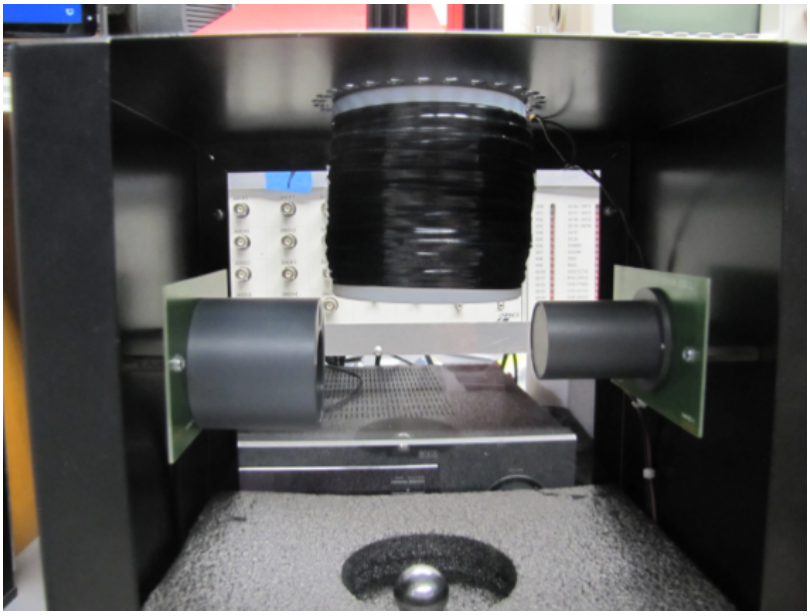

Figure 2: Parts of the Maglev System: the electromagnet (top), the photo-array sensor (sides), and the ball (bottom)

2.1.2 How the MagLev System Operates

The electromagnet generates a magnetic force, F_m given by the expression:

$$F_m = \frac{ki^2}{x^2} \tag{1}$$

where,

- i is the current of the coil
- x is the ball's vertical position
- k is a magnetic constant that will be determined experimentally.

Since gravity acts downwards with a force of mg, the resulting equation of motion becomes:

$$m\ddot{x} = F_m - mg, \tag{2}$$

which is nonlinear in both current and position. From equation 2 above and the lab manual, the equilibrium position, x_0 will only occur when the photo-array sensor voltage equals zero, corresponding to an equilibrium current, I_0, which will be delved into the later sections.

2.1.3 How the Sensor and Signal Flows in the Design

The sensor provides a voltage, V_{sensor}, that is related to the vertical position of the ball. This voltage is read through the NI DAQ and is compared to a desired set point. The error signal (the difference between the desired and current position values) is then fed through a PID controller implemented in LabVIEW, which outputs a control voltage. This control voltage is what drives the current inside the MagLev unit, controlling the coil current and the magnetic force. This idea is of the closed-loop form illustrated as a simple block diagram in Figure 3 below (referenced from the lab manual).

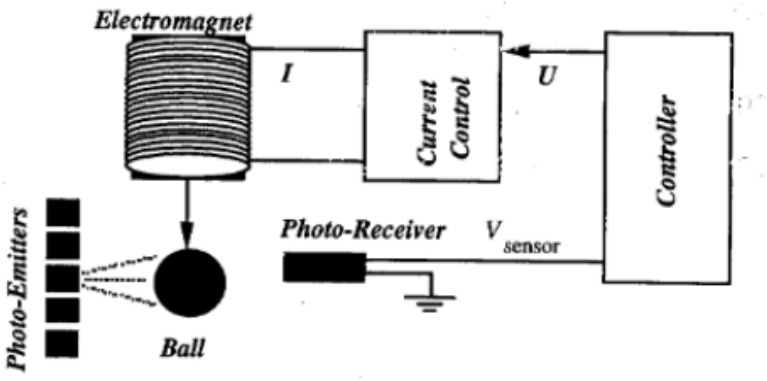

Figure 3: Simplified Diagram of the MagLev system

2.1.4 Closed-Loop Objectives

As mentioned earlier, due to the open-loop instability of the system, a PID controller will be needed. The PID must accomplish these goals:

- allows for the nonlinear dynamics around x_0,
- maintain stability,
- achieve acceptable transient response, and
- track the reference inputs well (height, sine, square, and random).

The linearization around x_0 is done because the system behaves approximately linearly in a small region around the equilibrium point.

2.2 Theoretical Background

In this section, a mathematical model of the Maglev system suitable for the controller design will be developed. From the reference manual, most of the math will be borrowed, but this lab will also build its own model and highlight some differences. It will begin by developing the nonlinear electromechanical description of the ball-magnet dynamics. Then, identify the equilibrium operating point and derive a linearized model and transfer function $G(s)$ for use in the design.

2.2.1 Derivation of the Nonlinear Dynamics

The vertical motion of the steel ball, as mentioned earlier, is governed by the balance between the gravitational force and the upward magnetic force. This is illustrated by the free-body diagram sketch in Figure 4 below. Applying Newton's second law

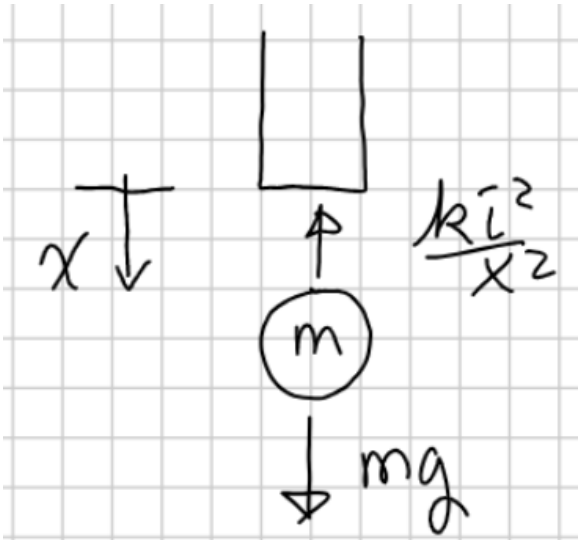

Figure 4: Free-body diagram of the ball-magnet interaction

in the vertical gives:

$$m\ddot{x} = F_m(i, x) - mg, \tag{3}$$

where m is the ball mass, x is the vertical distance between the ball and the electromagnet, i is the current in the coil, and g is the acceleration due to gravity. By substituting the magnetic force formula from equation (1) into equation (3), the nonlinear equation of motion becomes:

$$m\ddot{x} = \frac{ki^2}{x^2} - mg. \tag{4}$$

2.2.2 Equilibrium Operating Point

Equation 4 above needs to be linearized about the equilibrium point because it will be difficult to apply linear control principles, as the equation involves current (i) and position (x), which are nonlinear in both variables. At the nominal operating point, the ball levitates at a fixed position x_0 under a constant coil current I_0, and zero acceleration:

$$\ddot{x} = 0, x = x_0, i = I_0 \tag{5}$$

Now, substituting equation (5) into equation (4) gives:

$$0 = \frac{kI_0^2}{x_0^2} - mg \implies \frac{kI_0^2}{x_0^2} = mg. \tag{6}$$

Therefore, the constant k can be expressed as:

$$k = \frac{mgx_o^2}{I_0^2} \tag{7}$$

2.2.3 Linearization about the Equilibrium Point

To linearize, small deviations are introduced near the equilibrium nominal operating point:

$$x = x_0 + \Delta x, i = I_0 + \Delta i, \tag{8}$$

where Δx is a small displacement of the ball from the equilibrium position and Δi is a small deviation of the coil current from the equilibrium current value. From the reference manual, equation (8) is then substituted into equation (4) to get:

$$m(\ddot{x_0 + \Delta x}) = mg - \frac{k(I_0 + \Delta i)^2}{(x_0 + \Delta x)^2} \tag{9}$$

By using Taylor's expansion on equation (9) and simplifying, the equation of motion becomes:

$$m\ddot{\Delta x} = \frac{2mg}{x_0}\Delta x - \frac{2kI_0}{x_0^2}\Delta i \tag{10}$$

It is also known from the lab manual that the current i is related to the controller output voltage U by the expression:

$$i = 0.15U + I_0 \tag{11}$$

Therefore, from this expression in (11), it can be seen that:

$$0.15U + I_0 = I_0 + \Delta i \implies \Delta i = 0.15\Delta U \tag{12}$$

Equation (12) is then substituted into equation (10) to get the linearized form in terms of Δx and ΔU:

$$m\ddot{\Delta x} = \frac{2mg}{x_0}\Delta x - \frac{2kI_0 \cdot 0.15}{x_0^2}\Delta U \tag{13}$$

For the sensor, the relation in the lab manual will be reintroduced below:

$$V_{sensor} = -\gamma(x - x_0). \tag{14}$$

At equilibrium, $V_{sensor} = 0$, so the relation becomes:

$$\Delta V_{sensor} = -\gamma \Delta x \implies \Delta x = -\frac{\Delta V_{sensor}}{\gamma} \tag{15}$$

By substituting equation (15) into (13), we get a relationship in terms of ΔU and ΔV_{sensor}:

$$-\frac{m}{\gamma}\ddot{\Delta V_{sensor}} = -\frac{2mg}{\gamma x_0}\Delta V_{sensor} - \frac{2kI_0 \cdot 0.15}{x_0^2}\Delta U \tag{16}$$

2.2.4 Plant Transfer Function

Taking the Laplace of equation (16) with zero initial conditions gives:

$$\frac{m}{\gamma}s^2 V_s(s) = \frac{2mg}{\gamma x_0}V_s(s) + \frac{0.3kI_0}{x_0^2}U(s) \tag{17}$$

Note that $V_s = V_{sensor}$ here. Now rearranging and simplifying,

$$(s^2 - \frac{2g}{x_0})V_s(s) = \frac{0.3kI_0\gamma}{mx_0^2}U(s) \tag{18}$$

Therefore, the plant transfer function (before the position sensor) after simplification can be expressed as:

$$G(s) = \frac{V_s(s)}{U(s)} = \frac{\eta}{s^2 - \omega_0^2}, \tag{19}$$

where:

$$\eta = \frac{0.3kI_0}{mx_0^2} = \frac{0.3g\gamma}{I_0} \tag{20}$$

and

$$\omega_0^2 = \frac{2g}{x_0} \tag{21}$$

The expression in equation (19) is a second-order approximation of the plant transfer function, with the input being the controller output voltage, $U(s)$, and the output being the sensor voltage, $V_s(s)$, fed into the position sensor. It can be seen that

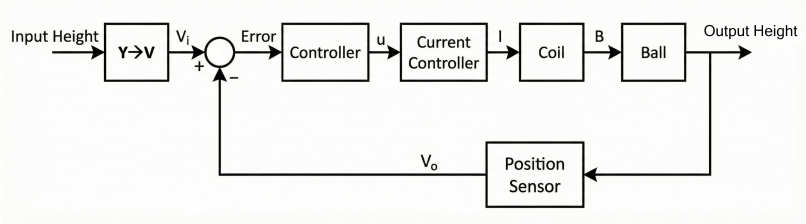

Figure 5: Theoretical block diagram of the overall system

the poles of equation(19) lie at $s = \pm\omega_0$. With one pole in the right-half plane (RHP), the Maglev plant is unstable and therefore needs a feedback control, which will be discussed in section 3. All of this is referenced from the block diagram of the controller-plant system drawn during our first checkpoint. It is shown in Figure 5 below: From Figure 5, it can be seen that the overall plant consists of the current controller, the electromagnetic coil, the ball, and the position sensor. However, the transfer function in equation (19) doesn't account for the position sensor. Hence, by taking the Laplace transform of equation (15), we get:

$$X(s) = -\frac{1}{\gamma}V_s(s) \implies \frac{X(s)}{V_s(s)} = -\frac{1}{\gamma} \tag{22}$$

Finally, by combining equations (19) and (22), the overall plant transfer function from the controller output $U(s)$ to the actual position $X(s)$ becomes:

$$G_{plant}(s) = \frac{X(s)}{U(s)} = \frac{V_s(s)}{U(s)} \cdot \frac{X(s)}{V_s(s)} = -\frac{\eta}{\gamma(s^2 - \omega_0^2)}, \tag{23}$$

with η and ω_0 having the same expressions as in equations (20) and (21), respectively. This plant transfer function $G_{plant}(s)$ together with the chosen PID controller $C(s)$ was used to specify the closed-loop dynamics illustrated by the block diagram in Figure 5. The tuning and design processes will be discussed in later sections, along with how they were used to predict steady-state error, transient response, and stability.

3 Procedures/Design Process

Obtaining Constants X_0, I_0, γ

The controller was determined using an iterative tuning process. The MagLev system is highly unstable without a controller, requiring careful tuning with specific constants to hover properly (I_0, X_0, γ).

To obtain the equilibrium position, X_0, a ruler was held by a clamp at a precise right-angle to the MagLev device's built-in scale. It was moved slowly until the sensor's

output voltage read 0 V on the LabView readout. This was then set as the zero point for all subsequent measurements.

To obtain the coil current I_0, the DC current required through the magnetic coil to hold the ball at X_0, Ohm's law was used. The MagLev device's manufacturer-specified coil resistance was $R_{coil} = 22\Omega$, and the voltage across the coil at this point was in the range of $13.4 - 14V$. Thus,

$$I_0 \approx \frac{V_{I0}}{R_{\text{coil}}},$$

which was computed to around $0.6A$

Finally, to obtain γ, the relationship between V_{sensor} and x was first approximated to be linear (i.e. the sensor voltage vs actual ball position). Then, using the same ruler-clamp method described above, several points close to X_0 were plotted with their corresponding V_{sensor} values, to a maximum of $\sim 10\,\text{mm}$ on either side of equilibrium. The slope of this line,

$$\gamma = \frac{\Delta V_{\text{sensor}}}{\Delta x},$$

was taken as the sensor gain used in our linear model.

Determining Controller Type and Tuning

Before a controller can be tuned, the type must be chosen and justified. The MagLev plant is open-loop unstable and linearized about an equilibrium operating point. A PID (proportional integral derivate) controller was chosen to control this system. This is primarily because of the highly unstable nature of the plant. The proportional action will stabilize the unstable plant, integral action will eliminate the steady-state position error, and derivate action will help damp the naturally undamped system. Additionally, PID controllers are simple to implement in LabView due to existing template files.

A PID controller takes the form of the equation below:

$$e(t) = r(t) - y(t) \tag{24}$$

$$u(t) = K_P\, e(t) + K_I \int_0^t e(\tau)\, d\tau + K_D \frac{de(t)}{dt} \tag{25}$$

Because the linearized MagLev model contains an unstable pole, the proportional term must be sufficiently large to shift the closed-loop poles into the left-half plane.

Thus, closed loop control is chosen over open loop control. The Laplace transform and closed loop transfer function can be found below.

$$C(s) = K_P + \frac{K_I}{s} + K_D s \tag{26}$$

$$\frac{X(s)}{U(s)} = \frac{C(s)\,G(s)}{1 + C(s)\,G(s)} \tag{27}$$

The values of K_P, K_I, and K_D are all chosen after tuning by the controls engineer.

Once the PID controller was selected, the tuning process could begin. The LabView VI, with guiding comments, can be seen in Figure 6 below.

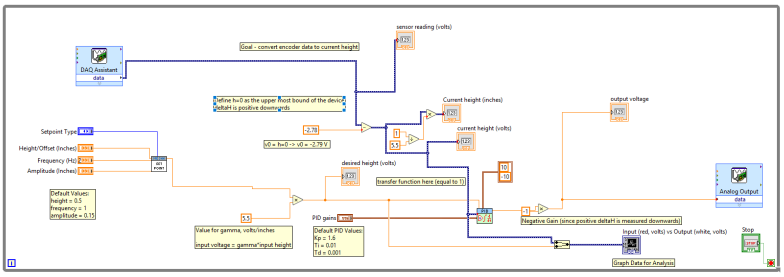

Figure 6: VI Screenshot (also in Appendix)

Regarding the VI, input height was measured as displacement from the top of the MagLev machine. This required the voltage to be translated by a set quantity, so that the translated voltage was equal to 0 when the height was equal to 0. Since the model can be approximated linearly, gamma scaling still applies. The V_0 setpoint was found to be $2.76V$. The translated voltage was then sent to the PID controller as the current voltage. The input height, in inches, is set by the user, and again is measured as displacement from the top of the MagLev machine. This value is then scaled by the experimentally found value of gamma, computed above and found to equal $\gamma = 5.5\frac{V}{in}$. This was sent to the PID controller as the desired voltage value. As proven above, near the equilibrium point the transfer function of the output voltage (coil voltage) over the input voltage (position sensor voltage value) was found to be equal to 1, so no additional scaling was needed. Coming out of the PID block, the output voltage is then scaled by -1. This is because all calculations assumed the global upwards direction to be positive, while our measred value of dispalcement assumed downwards to be positive.

In order to tune the PID, a desired height was chosen to be 0.5 inches. This number is very close to the equilibrium point of the device. A graphical interface was set up with real-time adjustable values for the PID. The PID block in LabView requires the

integral and derivative time constants, T_I and T_D, rather than the gain constants. The equations for their relationship can be found below:

$$K_I = \frac{K_P}{T_I} \tag{28}$$

$$K_D = K_P T_D \tag{29}$$

Manual tuning was selected instead of automatic tuning because the MagLev plant is physically open-loop unstable and sensitive to large control actions. Aggressive automatic methods, such as Ziegler–Nichols, can easily drive the system into saturation or cause the ball to fall. Manual P, D, I tuning allowed gradual stabilization while maintaining ball safety, decreasing time spent tuning, and ensuring the controller was tuned near the equilibrium point where the linear model is valid.

To begin tuning, all constants were set to equal zero. The proportional term, K_P, was slowly increased and the ball was being held in the MagLev machine near the equilibrium point. The goal was to have the ball feel like it was being tugged by the machine, but just at the point before the machine takes over and the ball attached to the top of the machine. It was quickly realized that it was near impossible to have a proportional only controller, as the unstable oscillations would pull the ball out of equilibrium and cause the controller to fail. Once the ball felt near weightless at equilibrium but still being held in the hand, a small amount of derivative T_D gain was introduced. This increased the damping of the system, preventing wild oscillations. Once the T_D term was, set, the ball was able to float in place with ease. One issue, however, was that the ball had an incorrect steady state. The T_I term was incrementally increased until the ball had no steady state error. The smaller the value of T_I, the smaller the rise time and settling time, but the larger the overshoot would be.

As can be seen in 7a, if $T_I = 0$, the model exhibits exceptional response to a change in input, in terms of settling time and rise time. It, however, has a very large and non-negligible steady state error. While this does not matter if the goal is to get the ball to hover or to respond well to the four test cases, this large error would at times push the ball outside of the working range of the device and cause it to fail. On the other side, 7b demonstrates a large value for T_I. Lots of overshoot is introduced, but the ball eventually settles to the desired input. This settling time, however, is unacceptable when testing the four cases, as the ball does not have enough time to reach steady state under quick frequencies such as the random value response or sinusoidal response. Through further testing, an acceptable value for T_I was determined, and the final values for all gains can be seen below.

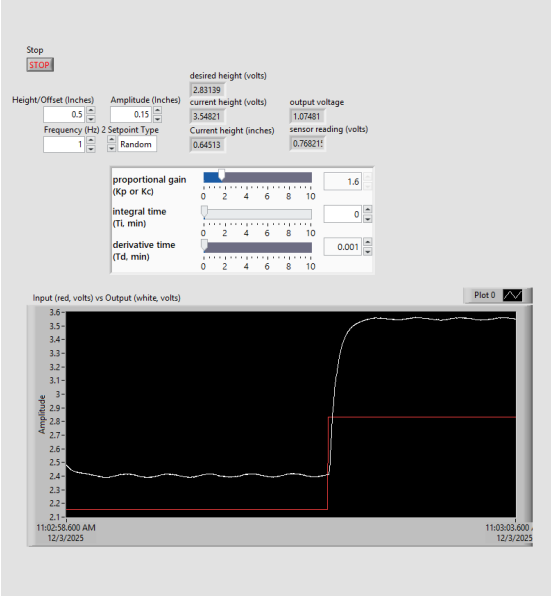

(a) Random input with $T_I = 0$

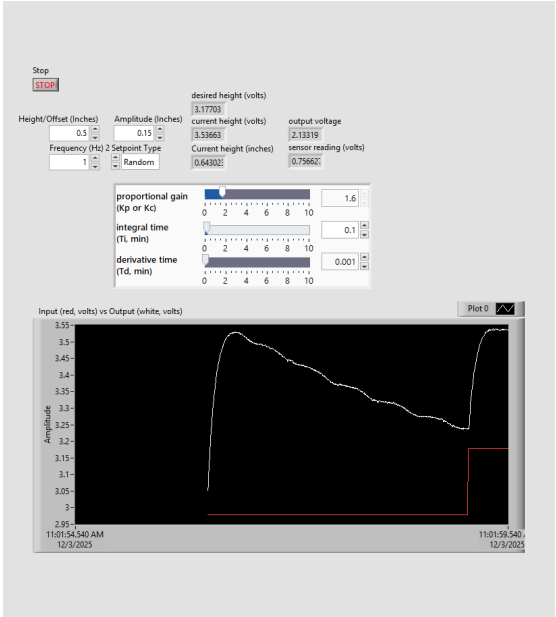

(b) Random input with $T_I = 0.1$

Figure 7: Random inputs with poor values of T_I

$$K_P = 1.6 \tag{30}$$

$$T_I = 0.01 \tag{31}$$

$$K_I = 160 \tag{32}$$

$$T_D = 0.001 \tag{33}$$

$$K_D = 0.0016 \tag{34}$$

After tuning, the controller was validated using the required input profiles: step, sinusoidal, square-wave, and random references. The system exhibited stable tracking, minimal steady-state error, and acceptable damping, confirming that the chosen gains satisfied the performance objectives while maintaining robustness near the operating point.

4 Results/Presentation Discussion

The controller was run with four input profiles: step, sinusoidal, square-wave, and random reference. In general, the controller exhibited exceptional performance and accuracy, especially considering the unstable nature of the system.

All tests were performed using the user interface found in Figures 8-11. The input height (in), the amplitude (in), and the frequency (Hz) are all manually controlled by the engineer. The PID terms K_P, T_I, and T_D are also inputted manually. A waveform chart displays both the desired voltage, in red, and the current voltage, in white, as a function of time. Additional variables are also displayed, primarily for debugging.

Constant Input

The first test run was the constant input test. A height is set by the user, measured as displacement from the top of the MagLev machine. The controller then attempts to hover the ball at the inputted height. Only heights near the equilibrium point can be chosen due to the unstable nature of the machine. A constant input of 0.5 inches can be seen below.

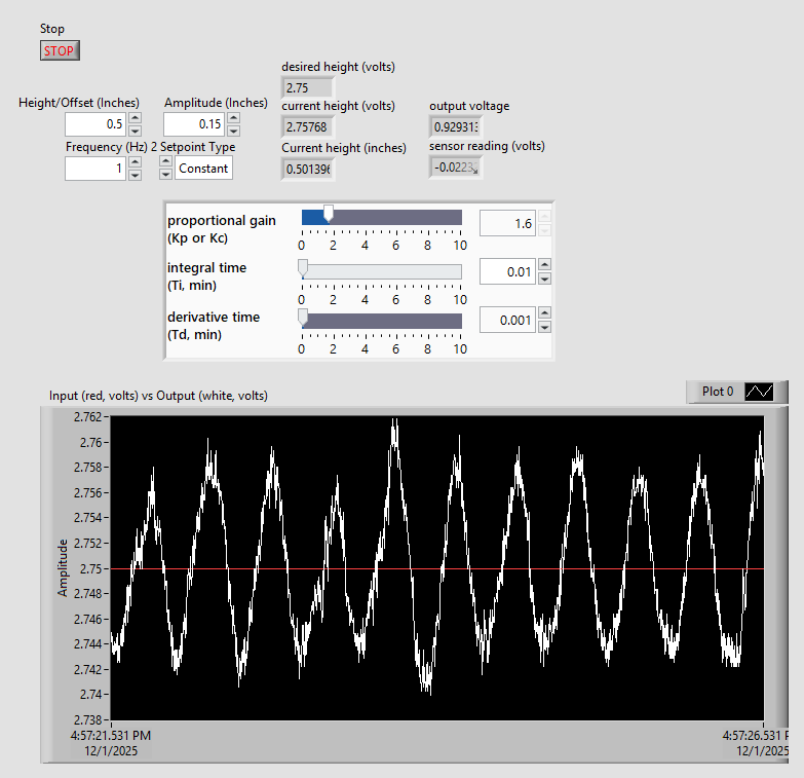

Figure 8: Constant input height settling time

As can be seen in Figure 8, the controller is able to capture the ball and hold it near the 0.5 inch setpoint, showing that the chosen PID gains stabilise the open-loop unstable plant. The output trace (white) tracks the input (red) with no divergence, indicating essentially zero steady-state error. Small underdamped oscillations are

present about the setpoint, though these are consistent with the tuning setup: the proportional term is large enough to keep the ball suspended, while the relatively small derivative term avoids excessive noise amplification at the expense of leaving some ripple. Overall, the response demonstrates that the controller meets the basic requirement of stable hovering at a fixed height, though additional fine-tuning could further reduce the small oscillations.

Random Number

The second test run was the random number test. A range is set by the user, defined as the bounds between the inputted height plus/minus the amplitude. At a set interval, a new input height in the given range is chosen and the machine tries to move the ball to the chosen height. The results of this test at a height of 0.5 inches and an amplitude of 0.15 inches can be seen below.

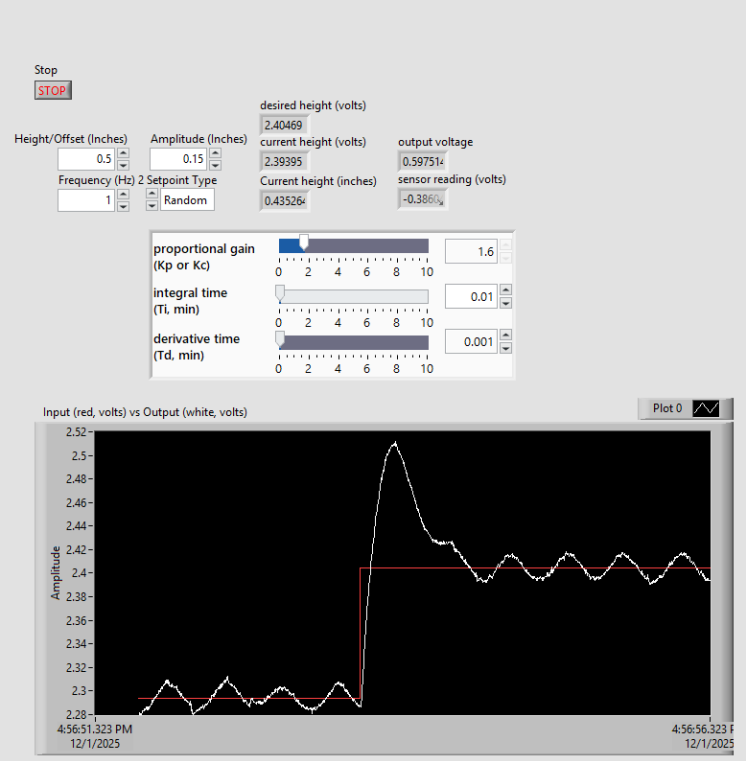

Figure 9: Random input heights

For the random-height test, Figure 9, the controller again keeps the ball near the set trajectory while it jumps unpredictably. The output (white) tracks the input (red) with a clear transient each time the setpoint moves: a noticeable overshoot appears after jumps, followed by a damped return to the new level. Once the transient dies

out, the steady-state error is small, indicating that the integral term is still effective even under changing commands. Compared to the constant-height case, the increased overshoot and ringing show the trade-off made during tuning between fast response and robustness on this inherently unstable plant, but the controller remains stable and responsive across the full random range.

Sinusoidal Input

The third test run was the sinusoidal test. A sinusodial input is created based on an input height, amplitude, and frequency. The results of this test at a height of 0.5 inches, amplitude of 0.15 inches and frequency of both 1 Hz and 2 Hz can be seen below.

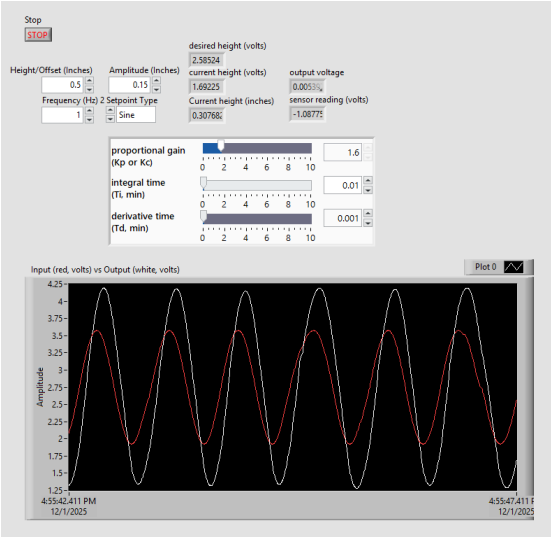

(a) Sine input with frequency = 1 Hz

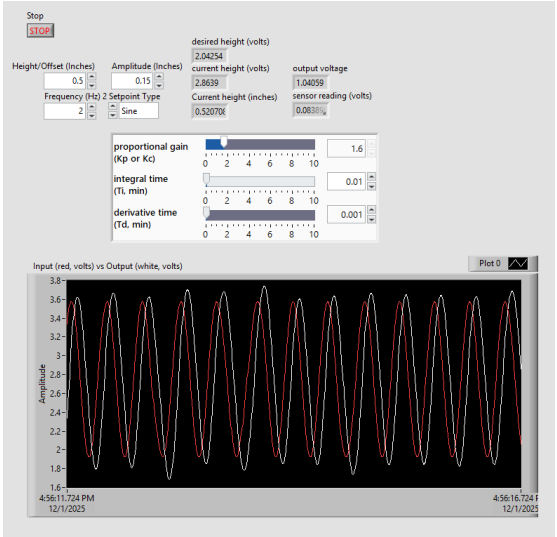

(b) Sine input with frequency = 2 Hz

Figure 10: Sine input tests at 1 Hz and 2 Hz

For the sinusoidal tests, the controller keeps the ball in a smooth periodic motion around the 0.5-inch offset and the output follows the commanded sine quite closely at both tested frequencies. At 1 Hz (Figure 10a), the output wave (white) is almost in phase with the input (red) but has a noticeably larger amplitude, indicating a closed-loop gain slightly greater than one at low frequency. At 2 Hz (Figure 10b), the output amplitude is more comparable to the input, with a similar small phase lag as at 1 Hz. Overall, the plots show that the tuned PID can track sinusoidal references well at least up to 2 Hz, with only small amplitude and phase shifts. This is consistent with a closed-loop bandwidth on the order of a few hertz.

Square Wave Input

The fourth test run was the square test. A square wave input is created based on an input height, amplitude, and frequency. The results of this test at a height of 0.5 inches, amplitude of 0.15 inches and frequency of both 1 Hz and 2 Hz can be seen below

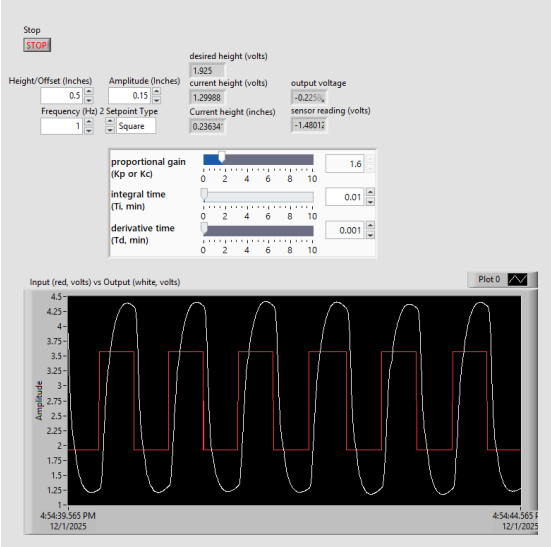

(a) Square input with frequency = 1 Hz

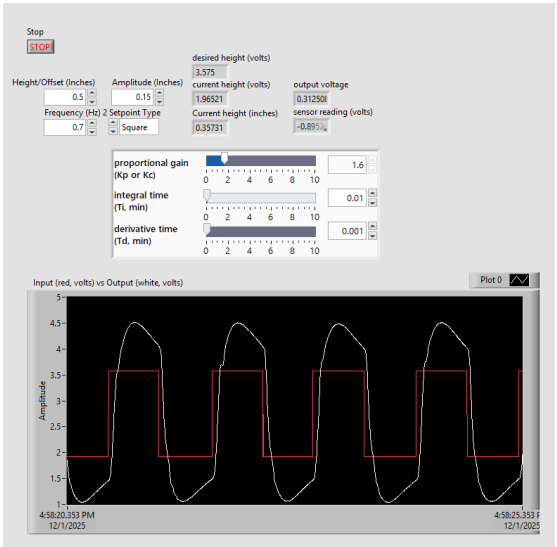

(b) Square input with frequency = 2 Hz

Figure 11: Square input tests at 1 Hz and 2 Hz

For the square-wave tests, the responses at 1 Hz and 2 Hz are qualitatively very similar. In both cases the controller cannot reproduce the sharp corners of the red reference, and instead the white output shows rounded, asymmetric pulses that overshoot the high and low levels and then drift back toward the plateau. At 2 Hz the overshoot is slightly smaller and the output hugs the reference levels a bit more closely, but the overall shape remains almost unchanged, which indicates that the system is still bandwidth-limited and underdamped for these square inputs. It tracks the average height well but cannot track rapid, discontinuous commands without distortion.

Oral Presentation Results

The in-lab oral presentation went smoothly, with the behaviour for the constant, random, square, and sine inputs being as expected based on previous testing. The LabView and PID controller were well set up and displayed, both front and back view. Questions were answered correctly and completely.

5 Conclusion

To conclude, this project successfully modeled, designed, and implemented a closed-loop PID controller that stabilised the inherently unstable MagLev plant and levitated a steel ball near the linearised equilibrium height, all while tracking constant, sinusoidal, random, and square-wave inputs. The nonlinear model and its linearisation about (X_0, I_0) produced a second-order plant with an unstable pole that agreed with observed behavior and provided a practical basis for controller design and tuning. The final gains yielded near-zero steady-state error for constant commands and good tracking of slowly varying inputs, with acceptable overshoot and damping given the physical constraints of the hardware. The primary fallbacks were residual oscillations and limits that prevented the controller from reproducing sharp corners in the square-wave tests. To improve, we would place greater emphasis on systematic, model-based tuning in simulation before lab implementation, tighter integration of data logging and analysis with the LabVIEW interface, and earlier iteration on UI layout and test procedures to more efficiently satisfy the performance and reporting expectations outlined in the project guidelines.

References

[1] M. Gustafson, E. Lipp, E. Stach, *et al.*, *ME 344 MagLev Control Project Manual*. Duke University, Fall 2025. MagLev F25 rev1.

A Milestones and Activity Log

Table 1: Activity Log of each team member.

Name	Date	Activity	Duration
Whole group	10/29/2025	Drew the Theoretical block diagram	10:05AM-11:30AM
Whole group	11/05/2025	Learned how to operate the MagLev unit	10:05AM-11:15AM
Desmond	11/05/2025	Stared confirmation of math model	11:15AM-12:00PM
Alex	11/07/2025	Started building VI's	3 PM- 5 stPM
Whole group	11/12/2025	Determined γ and X_0	10:05AM-12:35PM
Pierre	11/12/2025	Remeasured γ and X_0 values	10 AM-11 AM
Alex	11/14/2025	Began fine-tuning process	2 PM-4 PM
Whole group	11/19/2025	Continued tuning process	10:05 AM- 12:35 PM
Whole group	11/28/2025	Started writing report	All day
Whole group	12/02/2025	Prepared for presentations	7PM-9PM
Whole group	12/05/2025	Finalized Report	All day

B LabVIEW VI

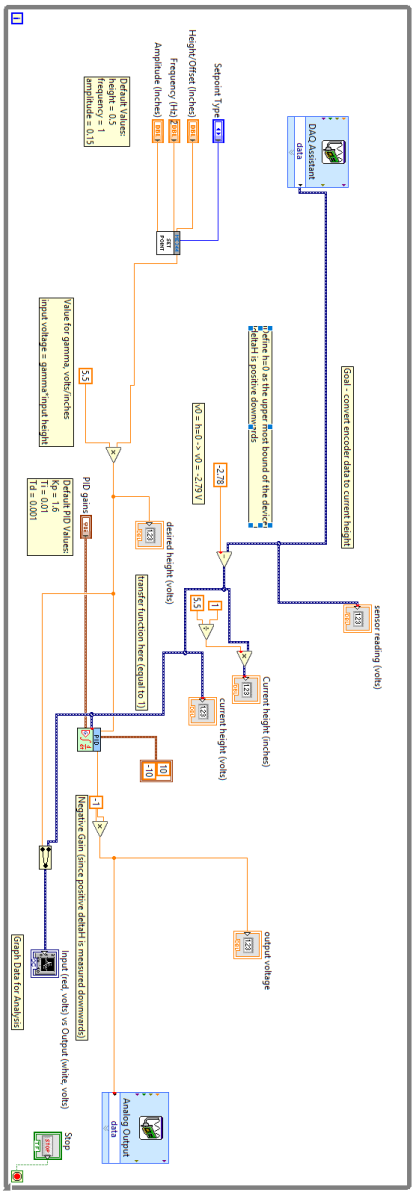

Figure 12: VI Screenshot (rotated)